Electrostatic Control of Phase Slips in Ti Josephson Nanotransistors

C. Puglia,[1,2] G. De Simoni,[2,*] and F. Giazotto[2,†]

[1] *Dipartimento di Fisica, Università di Pisa, Largo Bruno Pontecorvo 3, Pisa I-56127, Italy*

[2] *NEST, Istituto Nanoscienze-CNR and Scuola Normale Superiore, Pisa I-56127, Italy*

(Received 28 November 2019; revised manuscript received 27 February 2020; accepted 13 April 2020; published 11 May 2020)

The investigation of the switching-current probability distribution of a Josephson junction is a conventional tool to gain information on the dynamics of the phase slips as a function of the temperature. Here we adopt this well-established technique to probe the impact of an external static electric field on the occurrence of phase slips in gated all-metallic titanium (Ti) Josephson weak links. We show, in a temperature range between 20 and 420 mK, that the evolution of the dynamics of the phase slips as a function of the electrostatic field starkly differs from that observed as a function of the temperature. This fact demonstrates, on the one hand, that the electric field suppression of the critical current is not simply related to a conventional thermal-like quasiparticle overheating in the weak-link region. On the other hand, our results may open the way to operate an electrostatic-driven manipulation of phase slips in metallic Josephson nanojunctions, which can be pivotal for the control of decoherence in superconducting nanostructures.

DOI: 10.1103/PhysRevApplied.13.054026

I. INTRODUCTION

Although a static electric field is almost ineffective on the conduction properties of metals, recent experiments demonstrated the possibility of suppressing via conventional gating the critical current (I_C) of metallic Bardeen-Cooper-Schrieffer superconducting wires [1], Dayem bridges [2–5], and of proximity superconductor–normal-metal–superconductor (*S*-*N*-*S*) Josephson junctions (JJ) [6]. Yet, by means of a superconducting quantum interference device (SQUID) consisting of two gated Dayem-bridge constrictions, it has been possible to directly measure the impact of a static electric field on the quantum phase difference (ϕ) across a Josephson weak link [7]. The electric field was found to influence the SQUID current-phase relation via direct suppression of the critical current of a gated weak link. In addition, unexpectedly, phase shifts in the SQUID current versus flux relation were measured for gate-voltage values low enough to have no influence on I_C. Phase fluctuations present inside the superconductor [7] were shown to be a plausible cause for such an effect to occur, suggesting that the influence of the electric field on the phase may also lead to the occurrence of phase slips, i.e., local random 2π jumps of ϕ [8], which are responsible for the superconducting-to-normal state transition [9]. Phase-slip events, indeed, reflect into the value of the switching current (I_S), that is, when the bias current is swept from zero to above the critical current, the bias value at which the superconductor switches to the normal state. Due to the stochastic nature of phase-slip events, I_S statistically spreads around I_C, and its distribution [also known as the switching-current probability distribution (SCPD)] naturally provides information on the dynamics of the phase slips of mesoscopic superconducting devices [10–26] under the influence of external parameters such as, for instance, the temperature or an externally applied electric field. The latter was recently investigated in hybrid graphene-based Josephson junctions [27,28], but no relationship between the electric field and the SCPDs has been observed so far in genuine all-metallic superconducting systems. The relevance of such a topic lies in its natural link with the study of decoherence mechanisms in JJ devices, a matter of strong interest mainly in view of the realization of advanced superconducting quantum-information architectures. In this regard, we want to explicitly mention two superconducting qubit implementations that would benefit from a deep knowledge of the effect of electric fields on the dynamics of phase slippages in JJs: all-metallic transmons [29] and phase-slip qubits [30]. In the first case, the study of relation between electric field and SCPD is of great relevance because it allows us to identify and control one of the sources of phase decoherence related to the manipulation of the qubit state via field effect. In the phase-slip qubit case, the controlled generation of phase slips in a JJ is at the basis of the manipulation mechanism of the qubits. Therefore,

*giorgio.desimoni@sns.it

†francesco.giazotto@sns.it

the possibility to regulate the phase-slip rate, via a control electrode, provides a convenient knob for operating on a phase-slip qubit. We also highlight that, the control of the phase slips in a JJ is a tool to reduce, in binary-logic superconducting devices (see, e.g., Ref. [4]), the number of the errors due to the random transitions from the superconducting to the normal state.

Here we tackle the point of understanding the link between the application of a gate voltage and the occurrence of phase slippages in JJ, and report the investigation of SCPDs in electrostatically controlled titanium Dayem-bridge Josephson weak links in a temperature range from 20 to 420 mK, a regime explored so far only for Josephson tunnel junctions [32]. Our analysis of SCPDs of gated Dayem-bridge JJs demonstrates the dramatic action of the electrostatic field on the dynamics of the phase slips in metallic superconductors, and opens the way to operate an electric field-driven control of phase slips and, thereby, of decoherence in Josephson weak links. Moreover, we show that the evolution of SCPDs as a function of the electrostatic field starkly differs from that measured as a function of temperature. This fact indicates that the electric field-driven critical-current suppression is not related to a mere thermal-like quasiparticle overheating occurring in the junction region [33].

II. EXPERIMENT

A. Device nanofabrication

Our Ti-based Dayem-bridge weak links consist of 30-nm-thick, 150-nm-long, 120-nm-wide planar gated junctions fabricated by a single-step electron-beam lithography of a PMMA resist mask deposited onto a sapphire (Al_2O_3) single-crystal wafer with a nominal resistivity larger than 10^{10} Ω cm. Titanium is evaporated at a rate of 1.2 nm/s in an ultrahigh vacuum electron-beam evaporator with a base pressure of approximately 10^{-11} Torr. The 140-nm-wide gate electrode is separated by a distance of about 80 nm from the Dayem-bridge constriction. Figure 1(a) shows the false-color scanning electron micrograph of a representative Josephson device.

B. Low-temperature preliminar electric characterization

The low-temperature electric characterization of the devices is obtained by standard dc four-wire current versus voltage (I vs V) technique in a filtered cryogen-free ^{3}He $-^4$He dilution refrigerator, carried out with a low-noise current generator and room-temperature differential voltage preamplifier. Figure 1(b) shows the back and forth I vs V characteristics of a typical JJ device registered at several

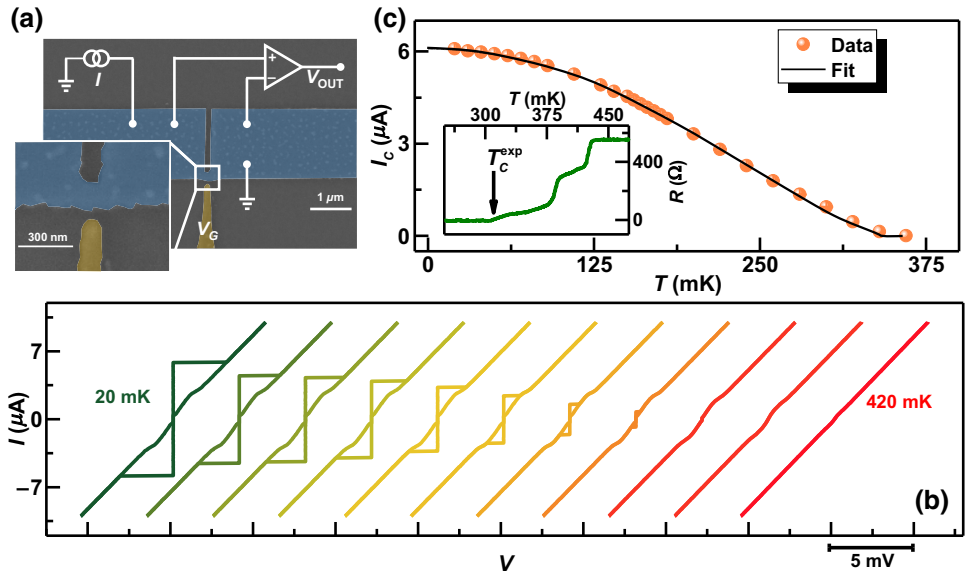

FIG. 1. (a) False-color electron micrograph of a typical Ti Dayem-bridge Josephson transistor. The Josephson weak link (inset) is current biased, and the voltage drop is measured with a room-temperature voltage preamplifier, while the gate voltage (V_G) is applied to a side gate electrode (yellow). (b) Back and forth current I versus voltage V characteristics of a representative device measured at different bath temperatures from 20 to 420 mK in steps of 40 mK. The curves are horizontally offset for clarity. (c) Evolution of the critical current I_C as a function of the temperature (dots). The dashed line represents the evolution of I_C according to Bardeen's theory [31]. The error bars on the measurement of I_C, calculated as the standard deviation σ of I_S over 10^4 samplings, is smaller than the size of dots in this scale. The inset shows the weak-link resistance (R) as a function of the bath temperature T. The estimated critical temperature ($T_C^{exp} \sim 310$ mK) is indicated by an arrow.

bath temperatures. The curves exhibit the conventional hysteretical behavior, which stems from heating induced in the weak link when switching from the dissipative to the dissipationless regime [34] (the device normal-state resistance is $R_N \simeq 550\ \Omega$). I_C decreases with temperature according to the behavior expected from Bardeen's formula [31] $I_C(T) = I_C^0\left[1-(T/T_C)^2\right]^{3/2}$, where I_C^0 is the zero-temperature critical current, and T_C is the critical temperature of the superconducting weak link. The fit of the I_C vs T characteristic with Bardeen's equation [shown as the black line in Fig. 1(c)] yields $I_C^{0\,(\mathrm{fit})} \simeq 6.02\ \mu$A and $T_C^{(\mathrm{fit})} \simeq 348$ mK. The latter value is in reasonable agreement with the critical temperature $T_C^{(\mathrm{exp})} \simeq 310$ mK extracted from the low-frequency lock-in resistance (R) versus T measurement [see the inset of Fig. 1(c)].

C. SCPD measurements

The stochastic behavior of the switching current of a Dayem bridge can be modeled with the resistively and capacitively shunted junction (RCSJ) theory [35,36], which schematizes a Josephson junction as the parallel of a resistor, a capacitor and a phase-dependent current generator $I(\phi)$. According to this model, we can interpret the transition to the normal state as a phase particle moving in a tilted-washboard potential under the effect of a friction force [see Fig. 2(a)] [37]. In this framework, switching events are represented by the escape of the phase particle from a minimum of the potential, corresponding to a 2π rotation in ϕ. The probability distribution $P(I,T)$ for this event to occur, as a function of the bias current I and of the electronic temperature T, is given by the inverse KFD transform [38,39]:

$$P(I,T) = \frac{\Gamma(I,T)}{\nu_I}\exp\left[-\frac{1}{\nu_I}\int_0^I \Gamma(I',T)dI'\right],$$

where

$$\Gamma(I,T) = \frac{L}{2\pi\xi(T)\tau_{\mathrm{GL}}(T)}\sqrt{\frac{\Delta U(I,T)}{k_BT}} \times \exp\left[-\frac{\Delta U(I,T)}{k_BT}\right]$$

is the phase-slip rate, $\nu_I = dI/dt$ is the ramp speed of the bias current, $\xi(T)$ is the Ginzburg-Landau (GL) coherence length, $\tau_{\mathrm{GL}}(T)$ is the so-called GL relaxation time [8], $\Delta U(I,T) = aE_J(T)\left[1-\frac{I}{I_C(T)}\right]^b$ is the height of the potential barrier, $E_J(T) = \hbar I_C(T)/2e$ is the Josephson energy, e

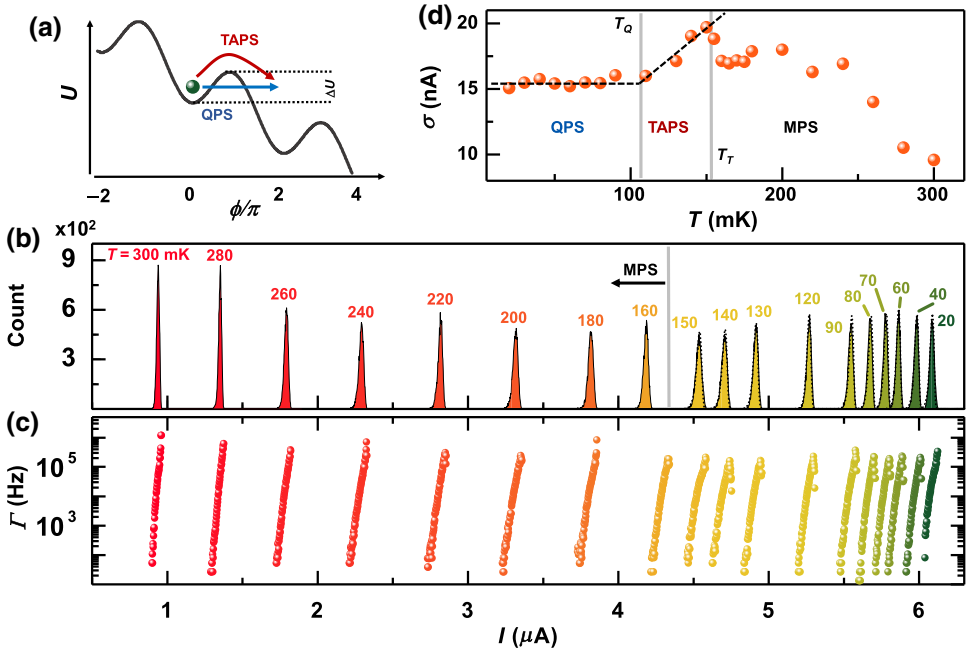

FIG. 2. (a) Schematic diagram of the tilted washboard potential showing the quantum phase-slip (QPS, blue arrow) and thermally activated phase-slip (TAPS, red arrow) processes. ΔU is the height of the barrier defined as the energy difference between a minimum and the following maximum of the washboard potential (black line). (b) Switching-current probability distributions versus current I obtained at different temperatures from 20 to 300 mK. Dotted lines represent the best-fit curves obtained with the Kurkijärvi-Fulton-Dunkleberger (KFD) model. The gray vertical line indicates the crossover temperature from TAPS to MPS regime. (c) Experimental rate Γ vs I obtained with the direct KFD transform for the same temperature values as in (b). (d) Standard deviation σ of the SCPDs versus bath temperature T. The crossover temperatures, $T_Q \simeq 110$ mK and $T_T \simeq 160$ mK, separate QPS-TAPS and TAPS-MPS regimes, respectively. For each SCPD the total sampling number of I_S is 10^4.

is the electron charge, and (a, b) are parameters accounting for the typology of the Josephson weak link [37]. Conventionally, the critical current I_C of the superconducting junction is assumed to be either the maximum current for which $P(I,T) \neq 0$ or the mode of the SCPD; in the following we adopt the latter definition.

1. Temperature dependence of SCPDs

Figure 2(b) shows the SCPDs built through 10^4 acquisitions of the switching current measured at several temperatures ranging from 20 to 300 mK. To perform SCPD measurements we use a 750-KHz bandwidth input-output analog-to-digital and digital-to-analog converter (ADC and DAC) board for the acquisition of the voltage drop signal and the generation of the bias current, respectively. The input signal consisted of an 8.7-Hz saw-tooth current wave obtained by applying a voltage signal generated by the digital board to an 1 MΩ load resistor. The current wave is composed by a positive linear ramp with amplitude 10 μA, and slope $v_I = 133$ μA/s followed by a 100-ms zero-current plateau, which turned out to be essential for the weak link to cool down between two consecutive transitions to the normal state. In particular, the mode of the distributions decreases by raising the temperature, as a consequence of the reduction of I_C. The width and the shape of the distributions follow the conventional behavior [37,40] as a function of the T, quantitatively described by the evolution of the standard deviation σ. Firstly, the quantum phase-slip (QPS) regime occurs when the transition from one minimum of the tilted-washboard potential to the next one is due to quantum tunneling. Since the tunneling process does not require an activation energy, the standard deviation of the SCPDs in this regime is expected to be temperature independent. The temperature range where tunneling is the main source of phase slips defines the so-called crossover temperature T_Q, above which $(T > T_Q)$ the thermal energy of the system allows the phase particle to hop over the potential barrier. In such a thermally activated phase-slip (TAPS) regime, the thermal energy supplied to the system grows with the temperature, resulting into a widening of σ as a function of T. Finally, when thermal energy is large enough to allow more than one phase-slip event to occur simultaneously $(T > T_T)$, the system falls in the so-called thermally activated multiple phase-slip (MPS) regime, and the standard deviation is known to decrease as a function of T [37].

The plot of σ vs T for the same Josephson nanotransistor, shown in Fig. 2(d), demonstrates that our Ti Dayem bridge follows the RCSJ model and the conventional phase-slip theory [37,41–43]. Indeed, from 20 up to 110 mK it shows an almost constant value of σ of approximately 15 nA (QPS regime), from 110 to approximately 150 mK the standard deviation is proportional to the temperature (TAPS regime), and for $T \gtrsim 150$ mK σ decreases down to approximately 10 nA at 300 mK (MPS regime). We wish to stress that the independence of σ in the QPS regime (i.e., $T \lesssim 110$ mK) cannot be ascribed to a saturation of the electronic temperature in the Josephson junction since the critical current turns out to increase in this range by decreasing T [see Fig. 1(c)]. Both in the QPS and TAPS regimes it is possible to fit the SCPD curves through the KFD transform [37,39,44] in order to extract the characteristic parameters of our system. Dotted lines in Fig. 2(b) represent the inverse KFD transform fits of our data, which show good agreement with the theory. Fit parameters, and a more detailed description about the fitting procedure are provided in the Appendix section.

Figure 2(c) shows the JJ escape rate $\Gamma(I,T)$ computed through the direct KFD transform [39,44]

$$\Gamma(I_N,T) = \frac{P(I_N,T)v_I}{1 - w\sum_{k=0}^{N} P(I_k,T)},$$

where w is the bin size of the $P(I,T)$ histograms, and $P(I_k,T)$ is the switching probability in the current interval $[kw,(k+1)w]$ with $k \in \mathbb{N}$. $\Gamma(I_N,T)$ provides a measure of the phase lifetime of our Dayem bridges, which spans between 1 μs ($\Gamma \sim 10^6$ Hz) and 10 ms ($\Gamma \sim 10^2$ Hz). The above escape rate range is in agreement with conventional switching-current experiments performed so far [11,37].

2. Impact of the electrostatic field on SCPDs

Let us now focus on the characterization of the impact of the electrostatic field on the dynamics of the phase slips. To verify the customary [1,3,4,6,7] dependence of I_C on the electric field, a detailed measurement of $I_C(V_G)$ as a function of bath temperature is preliminary performed on our Dayem bridge [see Fig. 3(d)]. The curves turn out to be symmetric for $V_G \to -V_G$, and show the expected monotonic suppression of the switching current, with full quenching at $|V_G^C| \simeq 34$ V. Moreover, as the temperature grows, we observe the typical [1,3,4,6,7] plateau widening for low V_G values. The current (I_L) flowing between the constriction and the gate electrode is also measured, and it is found to be at most $I_L^{\max} \simeq 15$ pA for $V_G = 34$ V, corresponding to a gate-bridge resistance $R_L \simeq 2.3$ TΩ. For a more comprehensive discussion on the effect of the gate current see the Appendix section.

In order to assess the impact of the electric field on the SCPDs, we acquire the distributions at 20 mK for several different values of V_G. First of all, we emphasize that the application of an electric field to the weak link dramatically deforms the shape of the SCPDs. In particular, as shown in Fig. 3(a), for $V_G < 8$ V the SCPDs cannot be distinguished from the zero-gate one whereas a tail at low-current values appears for $8 < V_G < 14$ V. Moreover, the SCPDs strongly widen for 14 V $< V_G <$ 24 V. Finally, for $V_G > 24$ V, the SCPDs turn out to narrow. The

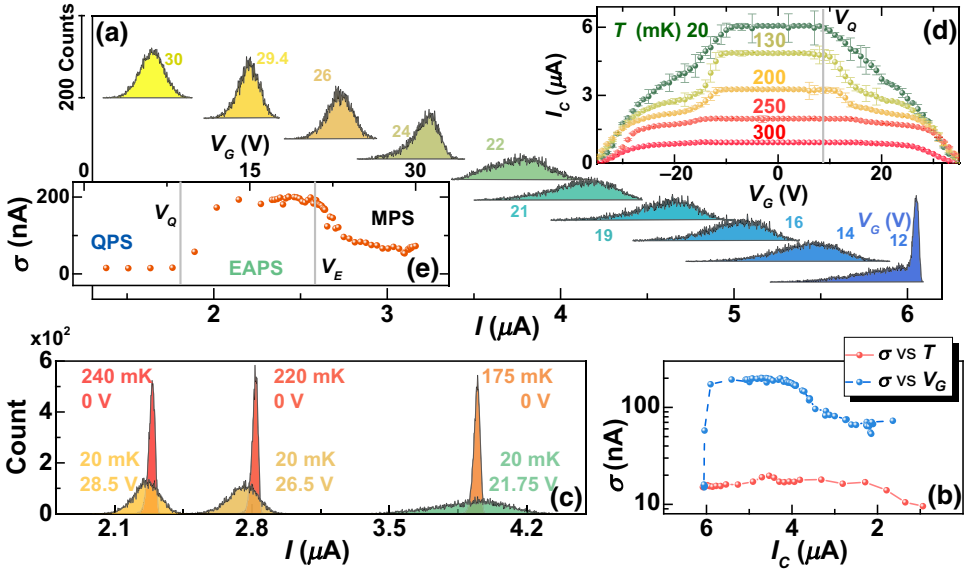

FIG. 3. (a) Switching-current probability distributions versus current I at different gate-voltage values from 12 to 30 V. The curves are vertically offset for clarity. (b) Comparison of σ vs I_C obtained for SCPDs as a function of temperature and $V_G = 0$ (light red), and of gate voltage at 20 mK (light blue). (c) Mode-matched SCPDs, red and orange distributions are obtained for $V_G = 0$ at selected temperatures whereas yellow and green distributions are measured at $T = 20$ mK for different gate-voltage values. (d) Dependence of the switching current I_C on V_G for different values of bath temperature from 20 to 300 mK. Data are obtained from the average computed over 25 acquisitions, and the error bars represent the standard deviation. The crossover voltage $V_Q \simeq 8V$ separates the QPS from the EAPS regime. (e) Standard deviation σ of the SCPDs vs V_G. Crossover voltages $V_Q \simeq 8V$ and $V_E \simeq 21V$ separate QPS-EAPS and EAPS-MPS regimes, respectively.

above behavior is quantitatively described by the standard deviation of the distributions displayed in Fig. 3(e). Here, we note that in the σ vs V_G curve it can still be identified as a region of constant standard deviation, thereby indicating a negligible contribution of the electric field to the phase slips for low V_G values. This behavior turns out to be equivalent to the QPS regime. Notably, such a regime occurs in the voltage range [i.e., $|V_G| < V_Q$, see Figs. 3(d) and 3(e)] where not even I_C is affected by the electrostatic field. For $|V_G| > V_Q$, I_C starts to monotonically decrease, phase slips are activated by the application of the electrostatic field, and σ grows with V_G obtaining its maximum value of approximately 200 nA. We define this region as the "electrically activated" phase-slip (EAPS) regime. This evidence suggests that, whatever the microscopic origin of I_C suppression, the latter is accompanied by a corresponding increase of phase-slip events.

Finally, for higher values of the electric field (i.e., $|V_G| > V_E \sim 20$ V), σ decreases and saturates to approximately 75 nA, a value that is around 7.5 times larger than the corresponding one in the high-temperature case. Therefore, this behavior, yet resembling the thermally activated MPS regime, *cannot* be ascribed to a conventional thermal trigger of phase slips. To emphasize this point, we compare the evolution of $\sigma(V_G, T = 20\ \text{mK})$ and $\sigma(V_G = 0, T)$ by plotting them versus their corresponding critical-current values [see Fig. 3(b)]. We speculate that the electric field effect is responsible for a deep modification of the weak-link phase dynamics by enhancing the switching probability (i.e., fluctuations) in a wider current bias range. In addition, although both σ vs T and σ vs V_G curves present a similar behavior, and three qualitatively similar regimes are recognizable in either curves, the average value of $\sigma(V_G)$ is around one order of magnitude larger than that of $\sigma(T)$.

To allow a further comparison between thermal and electric field distributions, we plot selected SCPDs corresponding to roughly the same I_C. Figure 3(c) shows such mode-matched distributions for $I_C = 2.2,\ 2.8,\ 4.0\ \mu$A. The I_C-matched distributions show markedly different shapes and widths, a behavior that might stem from electrostatically driven strong *nonequilibrium* induced in the superconducting Dayem bridge. Yet, this provides an additional confirmation that electrostatic field effect cannot be explained by a trivial local quasiparticle overheating of the superconductor. Indeed, assuming that the widening of the distributions are due to a thermal effect, the required effective quasiparticle temperature would be so high to be incompatible with the existence of superconductivity [45]. This observation reflects into a meaningless attempt to fit the electrically activated SCPDs with a conventional KFD transform since the necessary parameters would be totally outside the range of validity.

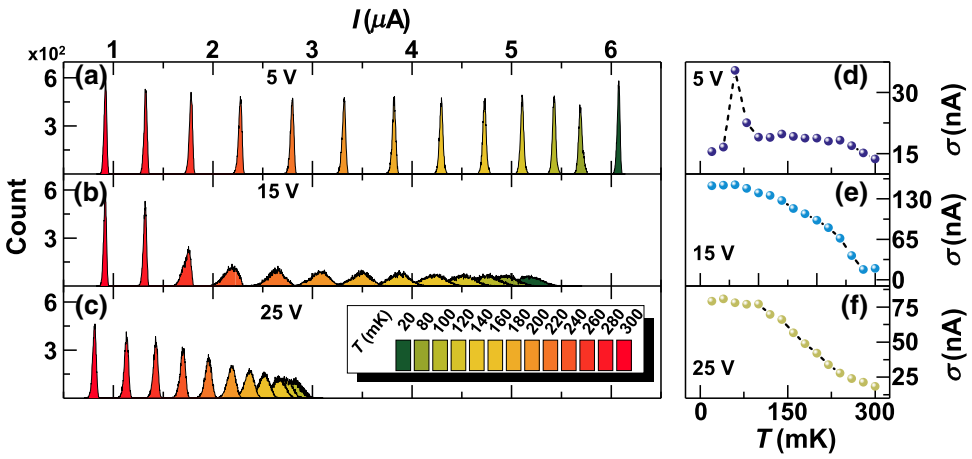

FIG. 4. (a)–(c) Evolution of the SCPDs from 20 mk to 300 mK for selected values of the gate voltage ($V_G = 5,\ 15,\ 25$ V). Widening of the SCPDs caused by the electric field is clearly visible. (d)–(f) Dependence of standard deviation σ on temperature T for the SCPDs shown in (a)–(c). The Josephson weak link turns out to evolve towards the MPSs regime as the electric field increases.

It is finally noteworthy to examine the response of the Josephson bridge under the simultaneous action of an electric field and thermal excitations. Figures 4(a)–4(c) show the SCPDs as a function of temperature in the range between 20 and 300 mK for $V_G = 5,\ 15,\ 25$ V, respectively. At high temperature, the distributions seem to recover the thermal behavior for each value of the applied electric field. Such an effect demonstrates a weakening of the electric field impact on phase slips at high temperature, which is consistent with what is already observed in previous experiments [1,3,4,6], and in our preliminary electric field characterization of the critical current [see Fig. 3(d)]. Nonetheless, the evolution of σ vs T drastically changes when the electric field is applied. Figures 4(d)–4(f) show the evolution of σ as a function of temperature for $V_G = 5,\ 15,\ 25$ V. At low values of the gate voltage (i.e., $V_G = 5$ V) we can identify QPS, TAPS, and MPS regimes [46]. By contrast, for $V_G \geq 15$ V, the electric field seems to drive permanently the JJ into a regime that is qualitatively similar to the thermal MPS regime for every temperature value. In such a configuration, QPS and TAPS regimes cannot be observed anymore.

III. CONCLUSIONS

In conclusion, we show the occurrence of different phase-slip regimes in a Ti Dayem-bridge Josephson weak link at several temperatures down to 20 mK. Firstly, the SCPDs of the system show the typical behavior as a function of temperature. Secondly, the distribution shape is largely affected by an externally applied electrostatic field. In particular, the standard deviation of the SCPDs far increases when the electric field is present. The drastic difference observed between the effect of the electric field and the temperature on SCPDs is a clear evidence of the *nonthermal* origin of the field effect-driven critical-current suppression, and can be ascribed to a strong nonequilibrium condition set in the weak link. Finally, as far as the specific applicative interest of the switching-current probability-distribution measurements presented in our paper is concerned, we stress that, especially in view of the possible realization of superconducting field effect-based qubits (such as, e.g., all-metallic gatemons) a good control and knowledge of phase noise and fluctuation sources in gated superconducting transistors is required. We conclude by highlighting that, in some sense, in our devices the gate voltage acts as an on-demand source of phase slippage in the Dayem bridge, which can be exploited to implement field-effect-based platforms of phase-slip qubits (see Ref. [30]).

ACKNOWLEDGMENT

We acknowledge A. Braggio, R. Citro, V. Golovach, S. Kafanov, N. Ligato, Y. Pashkin, F. Paolucci, P. Solinas, and E. Strambini for fruitful discussions. The authors acknowledge the European Research Council under the European Union's Seventh Framework Programme (COMANCHE; European Research Council Grant No. 615187) and Horizon 2020 research and innovation program under Grant Agreement No. 800923 (SUPERTED) for partial financial support.

APPENDIX

1. Gate-Dayem bridge current

The current between the Dayem-bridge (DB) constriction and the gate is measured by a standard two-probe technique with a low-noise voltage generator and a room-temperature current preamplifier. Figure 5(a) shows the I_C vs V_G characteristic for $T = 20$ mK from -35 to 35 V. The corresponding gate-Dayem-bridge current I_L [see Fig. 5(b)] as a function of V_G displays, in agreement with the conventional theory for electron tunnel injection at low biases [47], a linear behavior for almost the entire explored range, with a maximum value of $I_L^{\max} = 12.5$ pA at $V_G = 35$ V, which is on a par with previous similar experiments [1,3,4,6,7]. This measurement provides only an upper boundary for the current injected into or extracted from the DB: indeed, even neglecting leakages in the

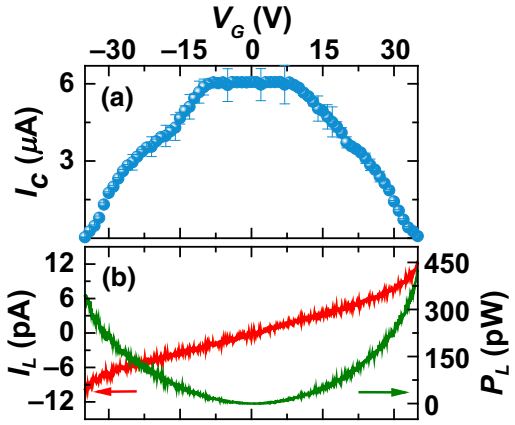

FIG. 5. (a) I_C vs V_G curve at a temperature of 20 mK for the same bridge device shown in the main text. Data are computed over 25 measure repetitions. (b) Leakage current I_L (orange line) and the corresponding Joule power P_L (green line) as a function of the gate voltage V_G measured at $T = 20$ mK. The resulting gate-channel resistance is $R_G = 2.54$ TΩ.

electrical setup lines, a fraction of I_L is expected to directly reach the leads. The green line in Fig. 5(b) represents the total power injected into the system. Its maximum, $P_L = 400$ pW, occurs for $|V_G| = 35$ V. We emphasize that such a power is unlikely to be directly dissipated into the weak link: the current between the gate and the DB can be described by the parallel of a possible diffusive current through the substrate and of a ballistic transport in the vacuum due to field emission at high electric fields, if present.

To correctly assess the impact of the diffusive current, it is necessary to take into account for the ratio N between the length of the shortest diffusive path connecting the gate and the DB ($d \sim 50$ nm) and the average scattering length in sapphire substrates ($\lambda_s \lesssim 0.1$ nm, see Ref. [48]), providing the average number of carrier collisions with phonons and defects. We stress that, in such a semiclassical approach, after each scattering event, the carrier motion is randomized. After that, it accelerates in the electric field, until it scatters again. Provided that in our devices $N \sim 500$, electrons and holes reach the Dayem bridge after having relaxed their kinetic energy several times. This suggests that such carriers are unlikely to have a role in raising the electronic temperature of the DB. Therefore, we believe that the diffusive current in the substrate cannot be taken as the origin the observed phenomenology.

We now focus on the process for which an electron is field emitted from the gate and absorbed by the Dayem bridge. An electron with an energy between 1 and 30 eV, and ballistically reaching the junction through the vacuum, releases its energy causing an abrupt increase of the electronic temperature. [33,45]. The electronic contribution to the heat capacitance C_e in a weak link in the normal state is

$$C_e = \Omega \times \gamma \times T_e,$$

where Ω is the volume of the junction, $\gamma = \pi^2 k_B^2 \nu_F/3$ is the Sommerfeld constant, $\nu_F = 1.35 \times 10^{47}\ \mathrm{m^{-3}\ J^{-1}}$ is the density of states at the Fermi level for Ti, and T_e is the electronic temperature of the system. The released energy $E(V)$ is proportional to the acceleration voltage (V) between the gate electrode and the Dayem bridge:

$$E(V) = q \times V,$$
$$P(t) = E\delta(t),$$

where q is the electron charge, δ is Dirac delta and $P(t)$ is the impulse power as a function of the time t. According to heat transport theory, the evolution of the electronic temperature in the junction is described by the following differential equation (see Ref. [45]), where T_B is the lattice temperature:

$$C_e \frac{\partial T_e}{\partial t} = P(t),$$
$$T_e = \sqrt{\frac{2E}{\Omega\gamma} + T_B^2} \sim 10\ \mathrm{K}.$$

We wish to stress that T_e is an underestimate of the final electronic temperature of the weak link because we assume C_e to be that of the normal state, which is typically exponentially larger than in the superconducting state owing to the presence of the energy gap in the density of states. The above calculation shows that a single electron with an energy about $E = 30$ eV injected into the Dayem bridge at $T_B = 10$ mK would raise its electronic temperature up to a value that is more than 20 times larger than its critical temperature ($T_C \simeq 300$ mK). This result allows us to make the statement that the heat originating from field-emitted electron absorption in the bridge cannot result in an equilibrium condition with a definite gate-controllable electronic temperature and critical current. Rather, we are forced to make the hypothesis that, due to continuous absorption of highly energetic electrons, the Dayem bridge bounces continuously between its normal and superconducting states. If this is the case, every time an electron is absorbed, it suddenly makes the bridge resistive, which then relaxes back to the superconducting state. The periodicity of such events is given by the electron emission rate, while the relaxation time is essentially given by the electron-phonon relaxation time, which is expected to be of the order of 1 ns (see Ref. [45]), i.e., much lower than the typical integration time of our measurement setup ($\simeq 20$ ms). In this scenario, during an I-V measurement, every time an electron is absorbed by the Dayem bridge when I is below the retrapping current (I_R) the variation of its

resistance is expected to be so fast to be undetectable with our setup. By contrast, when $I > I_R$, each time an electron is absorbed by the Dayem bridge, the latter should immediately switch to the normal state, and should persist in such a condition until the bias current is set back to 0. This implies that when field emission occurs the retrapping and the switching current should always coincide. Since this is not the case, we believe that we should exclude any hot-electron injection mechanism related to field emission as the predominant origin of our observations.

2. Inverse KFD transform fit

The fit is performed with the inverse KFD transform [37, 39,44]:

$$P(I,T) = \frac{\Gamma(I,T)}{\nu_I} \exp\left[-\frac{1}{\nu_I}\int_0^I \Gamma(I',T)dI'\right],$$

where $\nu_I = dI/dt$ is the ramp speed of the bias current, and $\Gamma(I,T)$ is the phase-slip rate, which assumes the following expression for the TAPS and the QPS regime, respectively:

$$\Gamma_{\mathrm{TAPS}}(I,T) = \frac{L}{2\pi\xi(T)\tau_{\mathrm{GL}}(T)}\sqrt{-\frac{aE_J(T)}{k_BT}\left[1-\frac{I}{I_C(T)}\right]^b}\exp\left\{-\frac{aE_J(T)}{k_BT}\left[1-\frac{I}{I_C(T)}\right]^b\right\},$$

$$\Gamma_{\mathrm{QPS}}(I,T,T_{\mathrm{QPS}}) = \frac{L}{2\pi\xi(T)\tau_{\mathrm{GL}}(T)}\sqrt{-\frac{aE_J(T)}{k_BT_{\mathrm{QPS}}}\left[1-\frac{I}{I_C(T)}\right]^b}\exp\left\{-\frac{aE_J(T)}{k_BT_{\mathrm{QPS}}}\left[1-\frac{I}{I_C(T)}\right]^b\right\},$$

where L is the geometric length of the weak link, $\xi(T)$ is the Ginzburg-Landau coherence length, $\tau_{\mathrm{GL}}(T)$ is the GL time constant, E_J is the Josephson energy, and a and b are parameters accounting for the typology of the Josephson weak link. Their values can be analytically derived for tunnel Josephson junctions ($a_{\mathrm{tunnel}} = 4\sqrt{2}/3$, $b_{\mathrm{tunnel}} = 3/2$) [37] and for long *metallic* superconducting wires ($a_{\mathrm{LW}} = \sqrt{6}$, $b_{\mathrm{LW}} = 5/4$) [10], but are not known for Dayem bridges, therefore they are left as free parameters of the fit. For all the fit of SCPD curves, a_{DB} and b_{DB} converged to the same values $a_{\mathrm{DB}} = 1.0 \pm 0.1$ and $b_{\mathrm{DB}} = 1.40 \pm 0.01$ Also, in the QPS regime (20 mK $\leq$ T $\leq$ 90 mK) we introduce the effective temperature T_{QPS} as a fitting parameter. The values for T_{QPS} yielded by the fitting procedure are shown in Table I. We note from the point of view of the Josephson coupling, our weak links are inbetween a tunnel junction and a long metallic superconducting wire just like the value found for parameter b_{DB} is inbetween the other types of junctions ($b_{\mathrm{LW}} < b_{\mathrm{DB}} < b_{S\text{-}I\text{-}S}$).

TABLE I. T_{QPS} values yielded by the fitting procedures of the SCPDs with the inverse KFD transform.

T (K)	T_{QPS} (mK)
0.02	99 ± 4
0.03	110 ± 5
0.04	114 ± 7
0.05	115 ± 6
0.06	119 ± 7
0.07	125 ± 9
0.08	135 ± 7
0.09	153 ± 8

3. Switching-current cumulative probability distributions

The switching-current cumulative probability distribution (SCCPD), or S curve, is defined as the integral of the switching-current probability distribution [22]. In this work, the S curves are obtained upon summation of the frequency counts of the SCPD histograms shown in the main text. The SCCPDs describe the probability to find the system in the normal state for a given value of the current bias.

Figure 6 shows the evolution of the SCCPD as a function of the temperature T ($V_G = 0$ V) and the gate voltage V_G ($T = 20$ mK). In particular, the application of the electric field results in a sizable widening of the S curves. A comparison between S curves with similar I_C values obtained in the thermal excitation case and in the electrostatic case allows us to appreciate how broader the SCCPDs are in the latter case. This fact is further evidence that field effect cannot be ascribed to a conventional "thermal-like" quasiparticle overheating in the weak-link region.

4. Characterization of a second Josephson Dayem bridge

In this section, we show the characterization of a Ti Dayem-bridge weak link similar to the one described in the main text. Qualitatively, the results obtained on this device

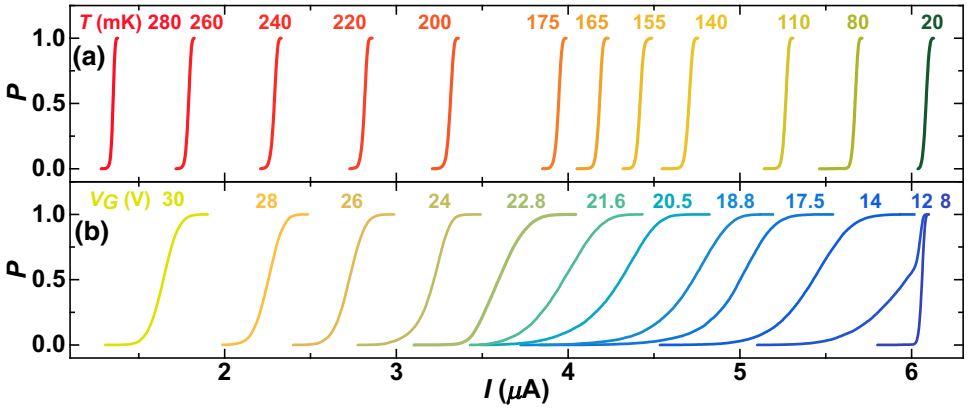

FIG. 6. (a) SCCPDs (S curves) as a function of the temperature from 20 to 280 mK. (b) S curves for different values of the gate voltage V_G from 8 to 30 V.

resembles those presented in the body of the manuscript. The thermal investigation of the system confirmed the typical behavior of this kind of weak link [3,35–37]. The preliminary characterization of I_S response to the electric field [see Fig. 7(a)] shows the nearly symmetric suppression [1,4–7] for both positive and negative gate-voltage values, with full quenching at $|V_G| \simeq 24$ V. More interesting is the evolution of the SCPDs as a function of the gate voltage V_G displayed in Fig. 7(b). As already similarly shown in the main text, the electric field modifies dramatically the shape of the SCPDs following the behavior described in the main body of the paper. Here, we note that the evolution of σ as a function of V_G [see Fig. 7(c)] clearly displays as well the three regimes of quantum phase slips, electrical activated phase slips, and multiple phase slips. To compare the thermal and electric field distributions, we plot selected SCPDs with almost mode-matched I_C. Figure 7(d) shows such distributions for $I_C = 0.9,\ 1.2,\ 1.9\,\mu$A. The I_C-matched SCPDs show drastically different shapes and widths.

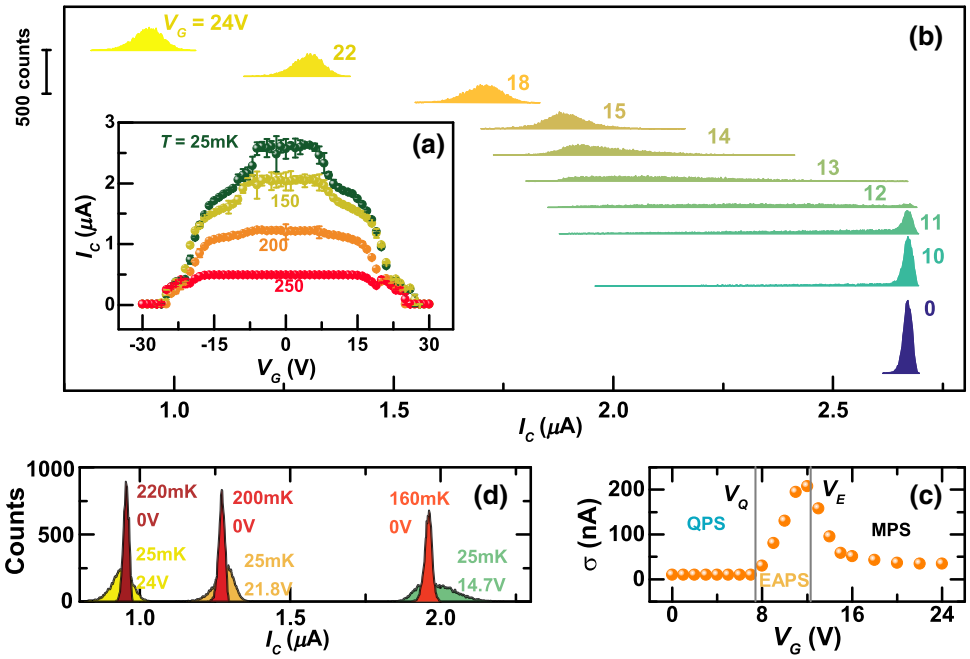

FIG. 7. (a) Dependence of the switching current I_C on V_G for different values of bath temperature from 25 to 250 mK. Data are obtained from the average computed over 25 acquisitions, and the error bars represent the standard deviation. (b) Switching-current probability distributions versus current I at different gate voltage values from 0 to 24 V. The curves are vertically offset for clarity. (c) Standard deviation σ of the SCPDs vs V_G. Crossover voltages $V_Q \simeq 8$ V and $V_E \simeq 12$ V separate QPS-EAPS and EAPS-MPS regimes, respectively. (d) Mode-matched SCPDs, red and orange distributions are obtained for $V_G = 0$ V at selected temperatures whereas yellow and green distributions are measured at $T = 20$ mK for different gate-voltage values.

[1] Giorgio De Simoni, Federico Paolucci, Paolo Solinas, Elia Strambini, and Francesco Giazotto, Metallic supercurrent field-effect transistor, Nat. Nanotechnol. **13**, 802 (2018).

[2] K. K. Likharev, Superconducting weak links, Rev. Mod. Phys. **51**, 102 (1979).

[3] Federico Paolucci, Giorgio De Simoni, Elia Strambini, Paolo Solinas, and Francesco Giazotto, Ultra-efficient superconducting Dayem bridge field-effect transistor, Nano Lett. **18**, 4195 (2018).

[4] Federico Paolucci, Giorgio De Simoni, Paolo Solinas, Elia Strambini, Nadia Ligato, Pauli Virtanen, Alessandro Braggio, and Francesco Giazotto, Magnetotransport Experiments on Fully Metallic Superconducting Dayem-Bridge Field-Effect Transistors, Phys. Rev. Appl. **11**, 024061 (2019).

[5] Federico Paolucci, Francesco Vischi, Giorgio De Simoni, Claudio Guarcello, Paolo Solinas, and Francesco Giazotto, Field-effect controllable metallic Josephson interferometer, Nano Lett. **19**, 6263 (2019).

[6] Giorgio De Simoni, Federico Paolucci, Claudio Puglia, and Francesco Giazotto, Josephson field-effect transistors based on all-metallic al/Cu/Al proximity nanojunctions, ACS Nano **13**, 7871 (2019).

[7] Federico Paolucci, Giorgio De Simoni, Paolo Solinas, Elia Strambini, Claudio Puglia, Nadia Ligato, and Francesco Giazotto, Field-Effect Control of Metallic Superconducting Systems, arXiv1909.12721 (2019).

[8] J. S. Langer and Vinay Ambegaokar, Intrinsic resistive transition in narrow superconducting channels, Phys. Rev. **164**, 498 (1967).

[9] William A. Little, Decay of persistent currents in small superconductors, Phys. Rev. **156**, 396 (1967).

[10] Mitrabhanu Sahu, Myung Ho Bae, Andrey Rogachev, David Pekker, Tzu Chieh Wei, Nayana Shah, Paul M. Goldbart, and Alexey Bezryadin, Individual topological tunnelling events of a quantum field probed through their macroscopic consequences, Nat. Phys. **5**, 503 (2009).

[11] Alexey Bezryadin, C. N. Lau, and M. Tinkham, Quantum suppression of superconductivity in ultrathin nanowires, Nature **404**, 971 (2000).

[12] Andrei D. Zaikin, Dmitrii S. Golubev, Anne van Otterlo, and Gergely T. Zimányi, Quantum Phase Slips and Transport in Ultrathin Superconducting Wires, Phys. Rev. Lett. **78**, 1552 (1997).

[13] Bum Kyu Kim, Hong Seok Kim, Yiming Yang, Xingyue Peng, Dong Yu, and Yong Joo Doh, Strong superconducting proximity effects in PbS semiconductor nanowires, ACS Nano **11**, 221 (2017).

[14] Jihwan Kim, Bum Kyu Kim, Hong Seok Kim, Ahreum Hwang, Bongsoo Kim, and Yong Joo Doh, Macroscopic quantum tunneling in superconducting junctions of β-Ag2Se topological insulator nanowire, Nano Lett. **17**, 6997 (2017).

[15] David Pekker, Nayana Shah, Mitrabhanu Sahu, Alexey Bezryadin, and Paul M. Goldbart, Stochastic dynamics of phase-slip trains and superconductive-resistive switching in current-biased nanowires, Phys. Rev. B **80**, 214525 (2009).

[16] U. C. Coskun, M. Brenner, T. Hymel, V. Vakaryuk, A. Levchenko, and Alexey Bezryadin, Distribution of Supercurrent Switching in Graphene under the Proximity Effect, Phys. Rev. Lett. **108**, 097003 (2012).

[17] Myung-Ho Bae, R. C. Dinsmore, M. Sahu, and Alexey Bezryadin, Stochastic and deterministic phase slippage in quasi-one-dimensional superconducting nanowires exposed to microwaves, New J. Phys. **14**, 043014 (2012).

[18] Andrew Murphy, Alexander Semenov, Alexander Korneev, Yulia Korneeva, Gregory Gol'tsman, and Alexey Bezryadin, Three temperature regimes in superconducting photon detectors: Quantum, thermal and multiple phase-slips as generators of dark counts, Sci. Rep. **5**, 10174 (2015).

[19] Xavier D. A. Baumans, Vyacheslav S. Zharinov, Eline Raymenants, Sylvain Blanco Alvarez, Jeroen E. Scheerder, Jérémy Brisbois, Davide Massarotti, Roberta Caruso, Francesco Tafuri, Ewald Janssens, Victor V. Moshchalkov, Joris Van de Vondel, and Alejandro V. Silhanek, Statistics of localized phase slips in tunable width planar point contacts, Sci. Rep. **7**, 44569 (2017).

[20] A. Murphy, P. Weinberg, T. Aref, U. C. Coskun, V. Vakaryuk, A. Levchenko, and A. Bezryadin, Universal Features of Counting Statistics of Thermal and Quantum Phase Slips in Nanosize Superconducting Circuits, Phys. Rev. Lett. **110**, 247001 (2013).

[21] Marek Foltyn and MacIej Zgirski, Gambling with Superconducting Fluctuations, Phys. Rev. Appl. **4**, 024002 (2015).

[22] MacIej Zgirski, M. Foltyn, A. Savin, K. Norowski, M. Meschke, and J. Pekola, Nanosecond Thermometry with Josephson Junctions, Phys. Rev. Appl. **10**, 044068 (2018).

[23] J. M. Kivioja, T. E. Nieminen, J. Claudon, O. Buisson, F. W. J. Hekking, and J. P. Pekola, Observation of Transition from Escape Dynamics to Underdamped Phase Diffusion in a Josephson Junction, Phys. Rev. Lett. **94**, 247002 (2005).

[24] M. Ejrnaes, D. Salvoni, L. Parlato, D. Massarotti, R. Caruso, F. Tafuri, X. Y. Yang, L. X. You, Z. Wang, G. P. Pepe, and R. Cristiano, Superconductor to resistive state switching by multiple fluctuation events in NbTiN nanostrips, Sci. Rep. **9**, 8053 (2019).

[25] Nayana Shah, David Pekker, and Paul M. Goldbart, Inherent Stochasticity of Superconductor-Resistor Switching Behavior in Nanowires, Phys. Rev. Lett. **101**, 207001 (2008).

[26] T. Aref, A. Levchenko, V. Vakaryuk, and A. Bezryadin, Quantitative analysis of quantum phase slips in superconducting Mo_76Ge_24 nanowires revealed by switching-current statistics, Phys. Rev. B **86**, 024507 (2012).

[27] Gil-Ho Lee, Dongchan Jeong, Jae-Hyun Choi, Yong-Joo Doh, and Hu-Jong Lee, Electrically Tunable Macroscopic Quantum Tunneling in a Graphene-Based Josephson Junction, Phys. Rev. Lett. **107**, 146605 (2011).

[28] Jae-Hyun Choi, Gil-Ho Lee, Sunghun Park, Dongchan Jeong, Jeong-O. Lee, H.-S. Sim, Yong-Joo Doh, and Hu-Jong Lee, Complete gate control of supercurrent in graphene p–n junctions, Nat. Commun. **4**, 2525 (2013).

[29] T. W. Larsen, K. D. Petersson, F. Kuemmeth, T. S. Jespersen, P. Krogstrup, J. Nygård, and C. M. Marcus, Semiconductor-Nanowire-Based Superconducting Qubit, Phys. Rev. Lett. **115**, 127001 (2015).

[30] J. E. Mooij and C. J. P. M. Harmans, Phase-slip flux qubits, New J. Phys. **7**, 219 (2005).
[31] John Bardeen, Critical fields and currents in superconductors, Rev. Mod. Phys. **34**, 667 (1962).
[32] James A. Blackburn, Matteo Cirillo, and Niels Grønbech-Jensen, Switching current distributions in Josephson junctions at very low temperatures, EPL (Europhys. Lett.) **107**, 67001 (2014).
[33] A. V. Timofeev, C. Pascual García, N. B. Kopnin, A. M. Savin, M. Meschke, F. Giazotto, and J. P. Pekola, Recombination-Limited Energy Relaxation in a Bardeen-Cooper-Schrieffer Superconductor, Phys. Rev. Lett. **102**, 017003 (2009).
[34] H. Courtois, M. Meschke, J. T. Peltonen, and J. P. Pekola, Origin of Hysteresis in a Proximity Josephson Junction, Phys. Rev. Lett. **101**, 067002 (2008).
[35] D. E. McCumber, Effect of ac impedance on dc voltage-current characteristics of superconductor weak-link junctions, J. Appl. Phys. **39**, 3113 (1968).
[36] W. C. Stewart, Current-voltage characteristics of Josephson junctions, Appl. Phys. Lett. **12**, 277 (1968).
[37] Alexey Bezryadin, *Superconductivity in Nanowires: Fabrication and Quantum Transport* (Wiley-VCH, Weinheim, 2012), p. 282.
[38] T. A. Fulton and R. C. Dynes, Switching to zero voltage in Josephson tunnel junctions, Solid State Commun. **9**, 1069 (1971).
[39] Juhani Kurkijärvi, Intrinsic fluctuations in a superconducting ring closed with a Josephson junction, Phys. Rev. B **6**, 832 (1972).
[40] D. E. McCumber and B. I. Halperin, Time scale of intrinsic resistive fluctuations in thin superconducting wires, Phys. Rev. B **1**, 1054 (1970).
[41] N. Giordano, Evidence for Macroscopic Quantum Tunneling in One-Dimensional Superconductors, Phys. Rev. Lett. **61**, 2137 (1988).
[42] N. Giordano and E. R. Schuler, Macroscopic Quantum Tunneling and Related Effects in a One-Dimensional Superconductor, Phys. Rev. Lett. **63**, 2417 (1989).
[43] H. A. Kramers, Brownian motion in a field of force and the diffusion model of chemical reactions, Physica **7**, 284 (1940).
[44] T. A. Fulton and L. N. Dunkleberger, Lifetime of the zero-voltage state in Josephson tunnel junctions, Phys. Rev. B **9**, 4760 (1974).
[45] Francesco Giazotto, Tero T. Heikkilä, Arttu Luukanen, Alexander M. Savin, and Jukka P. Pekola, Opportunities for mesoscopics in thermometry and refrigeration: Physics and applications, Rev. Mod. Phys. **78**, 217 (2006).
[46] Peng Li, Phillip M. Wu, Yuriy Bomze, Ivan V. Borzenets, Gleb Finkelstein, and A. M. Chang, Switching Currents Limited by Single Phase Slips in One-Dimensional Superconducting Al Nanowires, Phys. Rev. Lett. **107**, 137004 (2011).
[47] John G. Simmons, Generalized formula for the electric tunnel effect between similar electrodes separated by a thin insulating film, J. Appl. Phys. **34**, 1793 (1963).
[48] R. C. Hughes, Generation, transport and trapping of excess charge carriers in czochralski-grown sapphire, Phys. Rev. B **19**, 5318 (1979).